Nb Doping Strategy for Active Site Modification in Co_3O_4 to Enable Concurrent Hydrogen Production and Glycerol Valorization for Efficient Formate Production

Shobharajsinh Rathod[1], Kinjal K. Joshi[1], Pratik M. Pataniya[1], C. K. Sumesh[1], Sanni Kapatel[1,*]

[1]*Department of Physical Sciences, P D Patel Institute of Applied Sciences, Charotar University of Science and Technology, CHARUSAT, Changa-388 421, Gujarat, India*

*Corresponding Author Email: ***sannikapatel.phys@charusat.ac.in***

Supporting Note 1 (SN 1): Pre-treatment of nickel foam (NF)

Initially, the NF (3 cm x 3 cm) was sonicated for 10 min in acetone to remove organic contaminants, then for 10 min in 2.5 M HCl to remove the NiO layer on the upper surface. The NF was properly cleaned with deionized water for 15 min and dried for one hour at 60 °C.

Supporting Note 2 (SN 2): Material Characterizations

The crystal structure of NCO/NF was characterized by X-ray diffraction (XRD) using a D2 PHASER powder diffractometer (Bruker), equipped with Cu Kα radiation (λ = 1.541 Å). This technique provided essential insights into the crystalline phase of the material. The surface morphology and particle size distribution were analyzed using scanning electron microscopy (SEM, JEOL JSM-6010LA). To investigate the internal structure, particle arrangement, and crystallinity in more detail, transmission electron microscopy (TEM) was conducted with a JEOL JEM-2100 TEM operating at an accelerating voltage of 200 kV. The elemental composition and surface chemical states were examined using X-ray photoelectron spectroscopy (XPS) with a Thermo Scientific K-Alpha+ spectrometer, equipped with a monochromatic Al Kα source (hv = 1486.6 eV). The XPS spectra were collected at a 45° take-off angle, providing detailed information on the elemental distribution and oxidation states of the NCO/NF surface. In situ RAMAN analysis was performed using i-Raman Plus by A Metrohm Group of Company and Vionic powered by INTELLO by Metrohm Autolab.

Supporting Note 3 (SN 3): Product analysis.

The products of glycerol oxidation were analyzed using high-performance liquid chromatography (HPLC) and ^1H nuclear magnetic resonance (^1H NMR) spectroscopy. HPLC analyses were carried out using a Waters Alliance system (Model No. E2695) equipped with a quaternary gradient pump, degasser, autosampler, column oven, and a photodiode array (PDA) detector. Separation was achieved with a Shodex SH-1011 Sugar Column, using 0.1% (v/v) perchloric acid as the mobile phase at a constant flow rate of 1.0 mL min^{-1}. Each run was performed with an injection volume of 20 µL, while the column oven and autosampler were maintained at 50 °C and 25 °C, respectively. Chromatograms were recorded at 215 nm and processed with Empower 3 software, with a total run time of 24 minutes per sample.

The reaction products were identified by matching the retention times of the elution peaks with those of formic acid standards. Quantification was carried out using calibration curves generated from standard solutions of known formic acid concentrations.

Supporting Note 4 (SN 4): Faradaic efficiency calculation

The Faradaic efficiencies (FEs) of hydrogen (H_2) and formate were determined based on the total charge transferred during electrolysis and the experimentally measured products.

For hydrogen, the FE was calculated as:

$$FE = \frac{V(H_2)}{V_m * Q/nF} \times 100\% \quad \text{Eq-S1}$$

where V (H_2) is the experimentally measured volume of H_2, Q is the total charge passed through the electrode during electrolysis, V_m is the molar volume of an ideal gas at standard temperature and pressure (22.4 L mol^{-1}), F is the Faraday constant (96,485 C mol^{-1}), and n is the number of electrons transferred per H_2 molecule (n=2)

For formate, the FE was determined as:

$$FE = \frac{C \times V \times n \times F}{Q} \times 100\% \quad \text{Eq-S2}$$

Where, C is the concentration of formate in the electrolyte (mol L^{-1}), V is the total electrolyte volume (L), n is the number of electrons transferred per mole of product (for formate, n=8/3), F is Faraday's constant (96,485 C mol^{-1}), Q_{total} is the total charge passed during electrolysis (C).

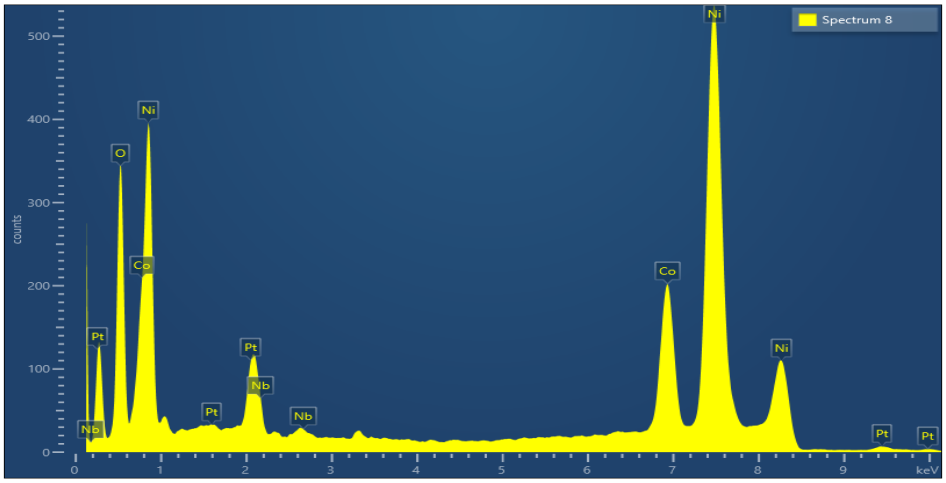

Figure S1 Energy-dispersive X-ray spectra (EDS)

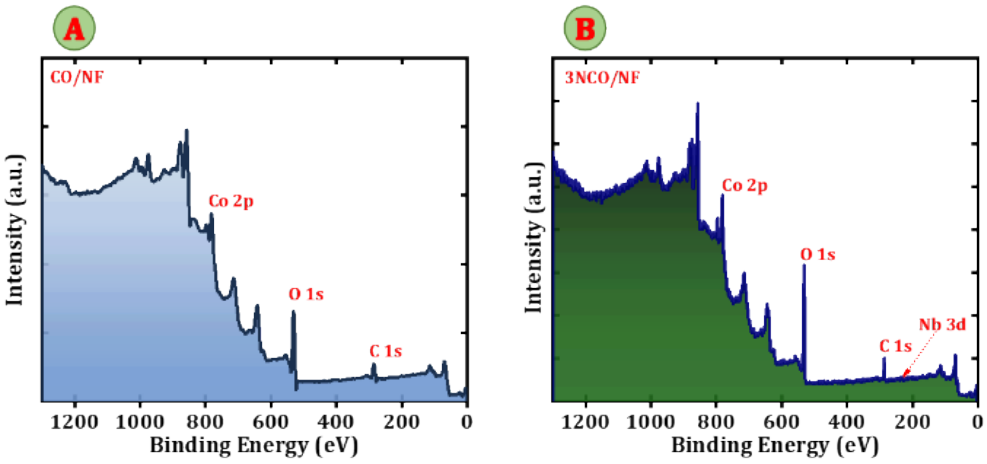

Figure S2 XPS survey scan of (A) CO/NF (B) 3NCO/NF

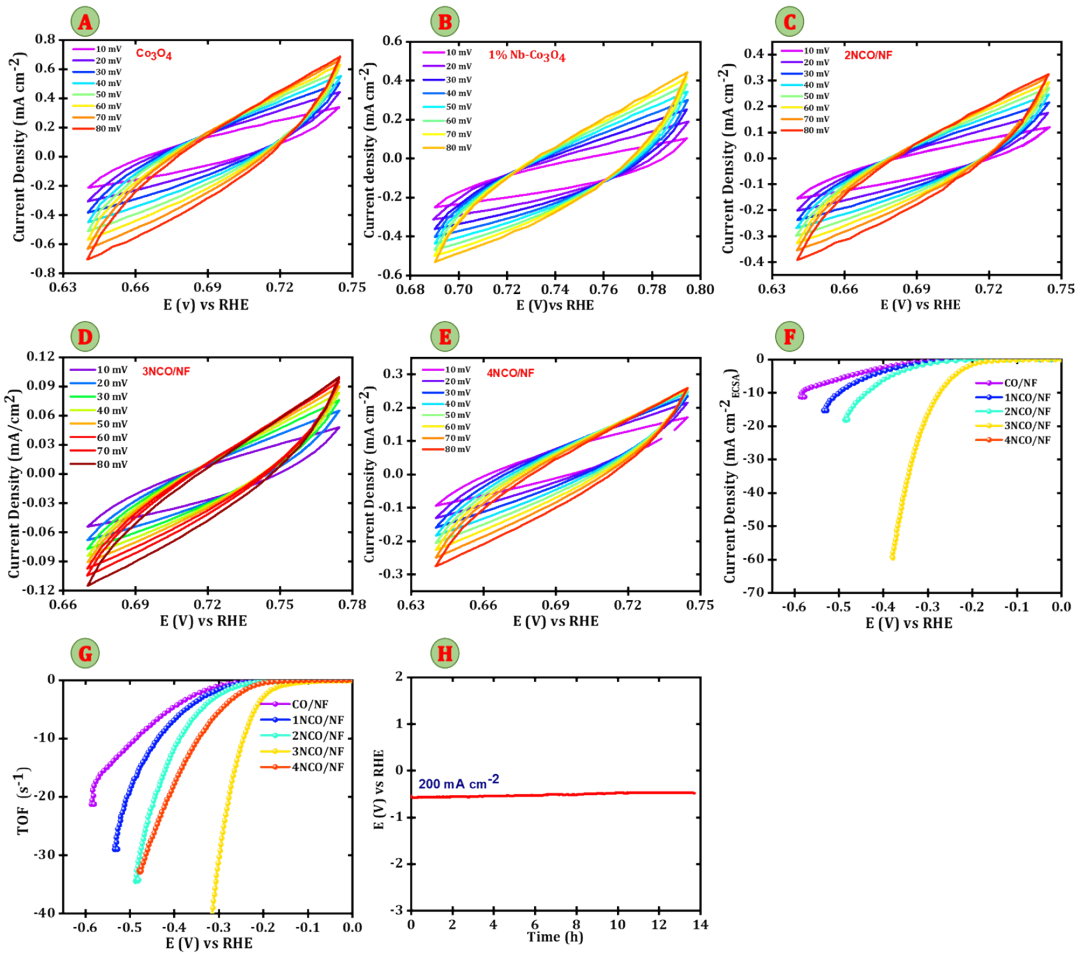

Figure S3 Cyclic voltammetry of (A) CO/NF, (B) 1NCO/NF, (C) 2NCO/NF, (D) 3NCO/NF, (E) 4NCO/NF, (F)Turnover Frequency vs potential plot, (G) ECSA normalization polarization curve, (H) Long-term stability by chronopotentiometry of 3NCO/NF in 1M KOH for HER.

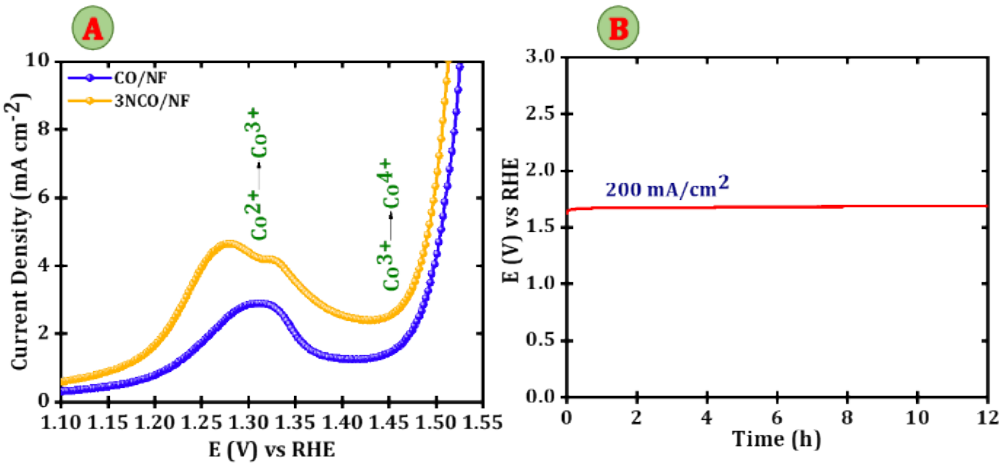

Figure S4 (A) polarization curve of CO/NF and 3NCO/NF at 5 mV s^{-1} (B) Long-term stability by chronopotentiometry of 3NCO/NF in 1M KOH for OER

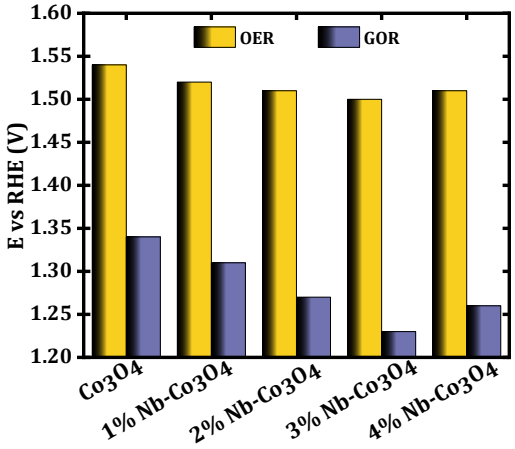

Figure S5 Overpotential comparison of OER and GOR at 10 mA cm^{-2}

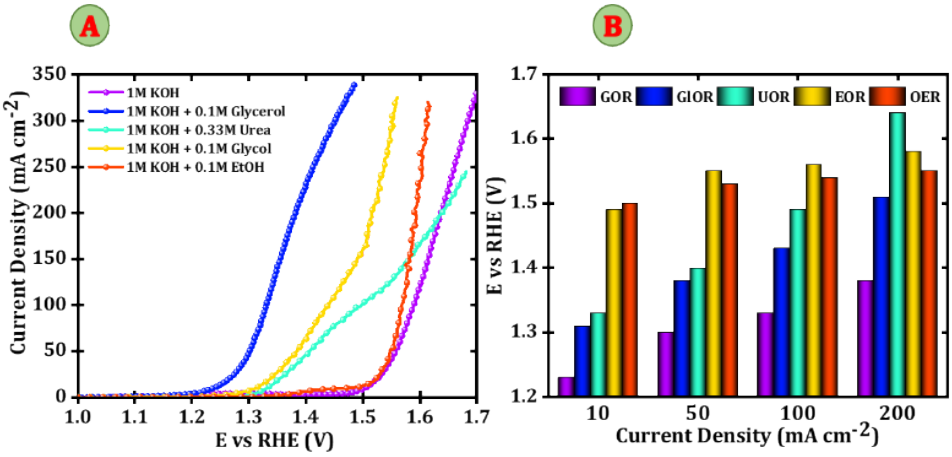

Figure S6 (A) Linear sweep voltammetry (LSV) curves of different alcohols (0.1 M) and urea (0.33M) in 1 M KOH, (B) Overpotential comparison of different alcohols at different current densities

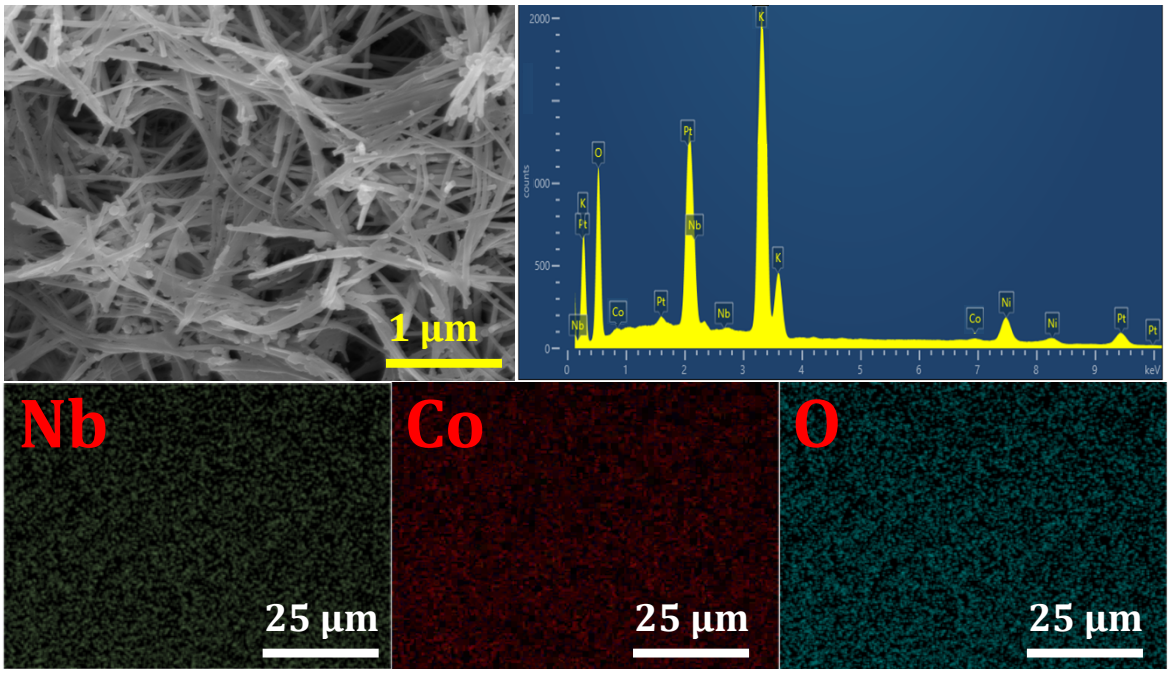

Figure S7 FESEM images and EDX mapping after the stability test in 1M KOH.

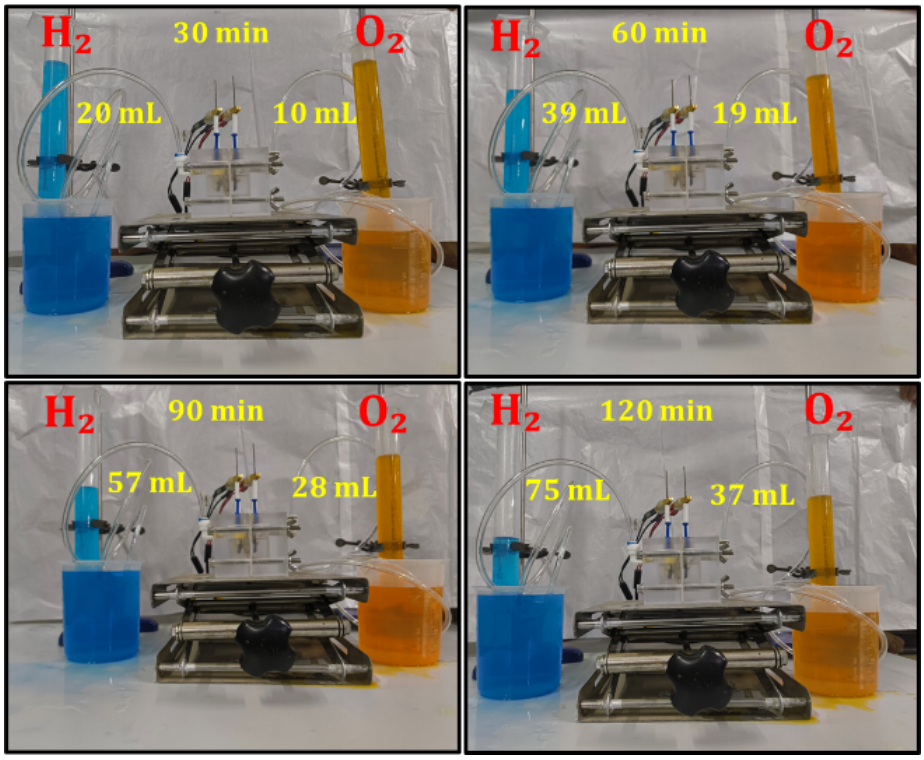

Figure S8 Digital photographs were captured at intervals of 30, 60, 90, and 120 minutes during the experiment to record the collection of hydrogen and oxygen gases.

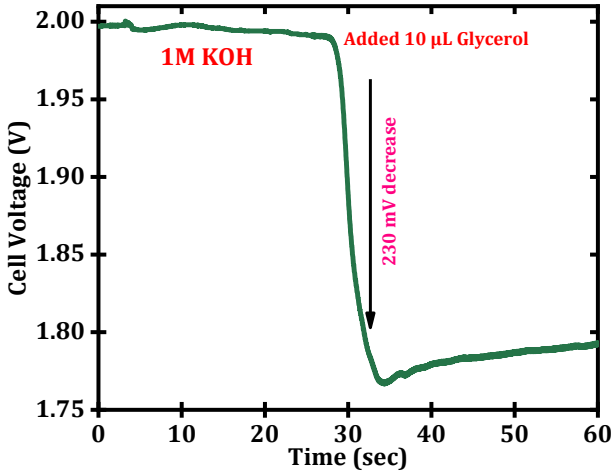

Figure S9. Chronopotentiometry measurements at a constant current density of 50 mA cm^{-2}

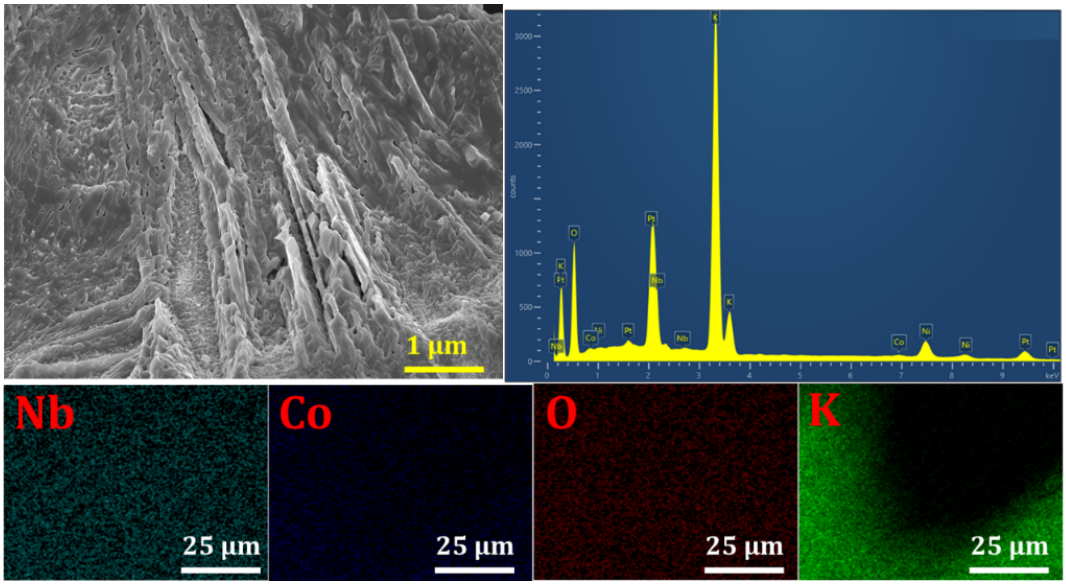

Figure S10. FESEM images and EDX mapping after the stability test in 1M KOH + 0.1M Glycerol

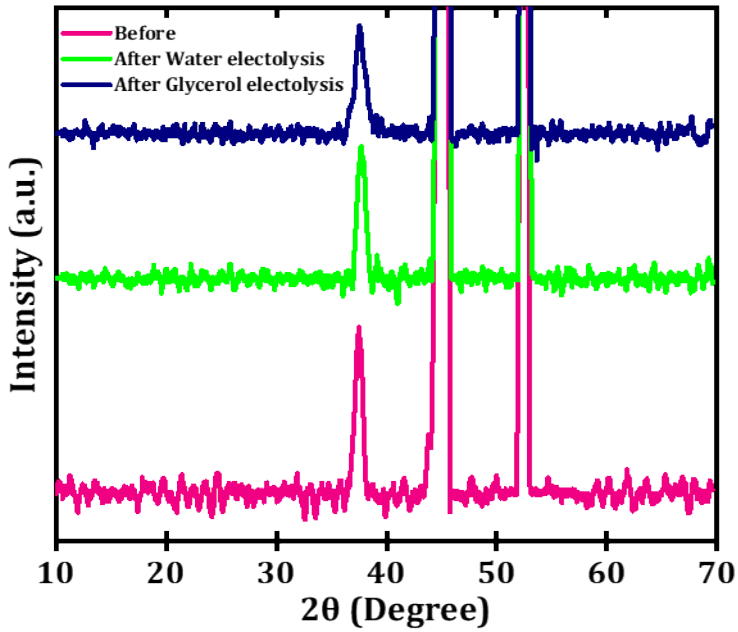

Figure S11 XRD patterns in 1 M KOH and 1 M KOH + 0.1 M glycerol electrolytes

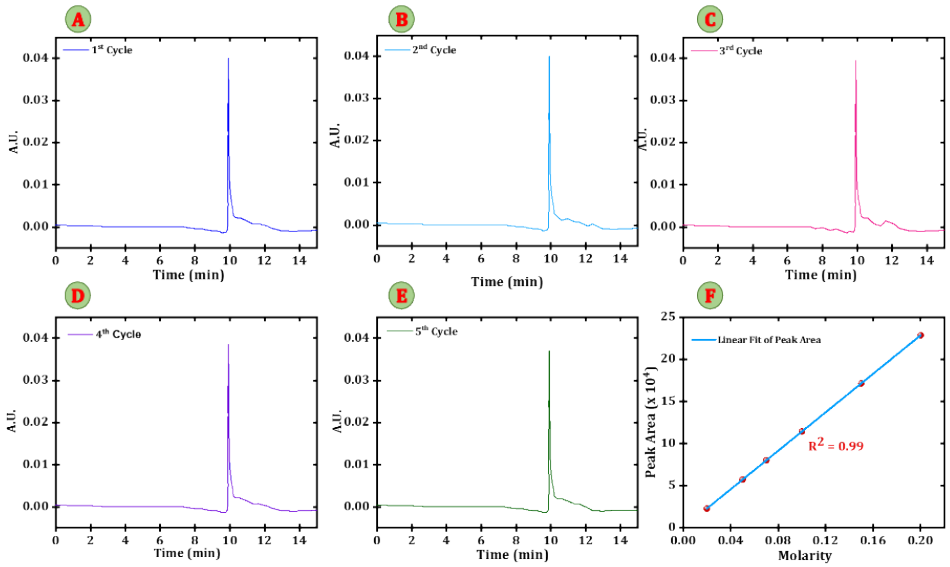

Figure S12 HPLC chromatograms (A–E) recorded after the 1st to 5th cycles, and (F) calibration curve for product quantification.

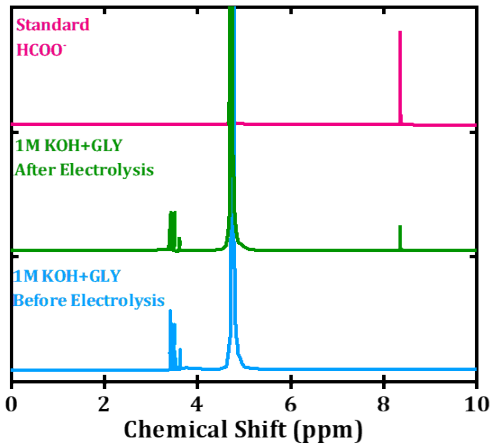

Figure S13 NMR spectra after 5th cycles

Supporting Note 5 (SN 5): Set-up for Solar-Driven Water Splitting

A solar-driven water-splitting experiment was conducted to assess the real-world applicability of the 3NCO/NF catalyst. A two-electrode electrolyzer was assembled with 3NCO/NF as both the anode and cathode, powered solely by a solar panel under natural sunlight. The electrolyte was 1 M KOH, and the electrochemical cell was enclosed to prevent thermal effects from direct solar heating. This setup successfully demonstrated the feasibility of using sunlight for water electrolysis, showcasing the 3NCO/NF||3NCO/NF system's potential for decentralized and sustainable hydrogen production.

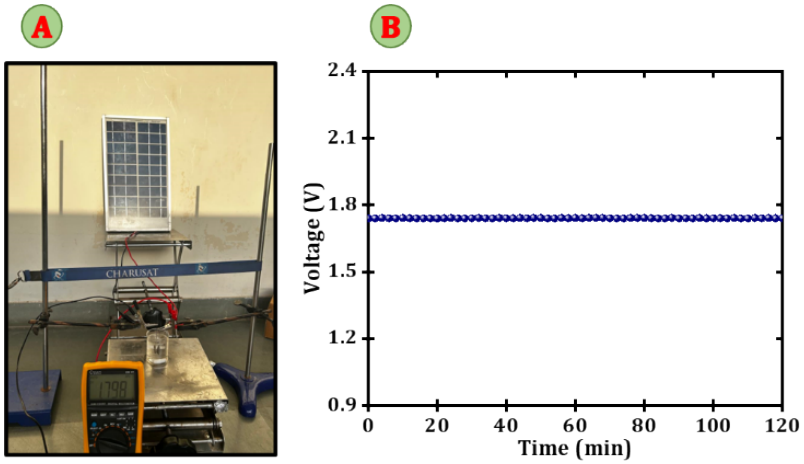

Figure S14 (A) Photograph of the experimental setup for the solar-driven water electrolyzer, and (B) Chronopotentiometric stability test of the 3NCO/NF||3NCO/NF solar-driven electrolyzer in 1 M KOH for 120 minutes, demonstrating a stable operating voltage under continuous solar illumination.

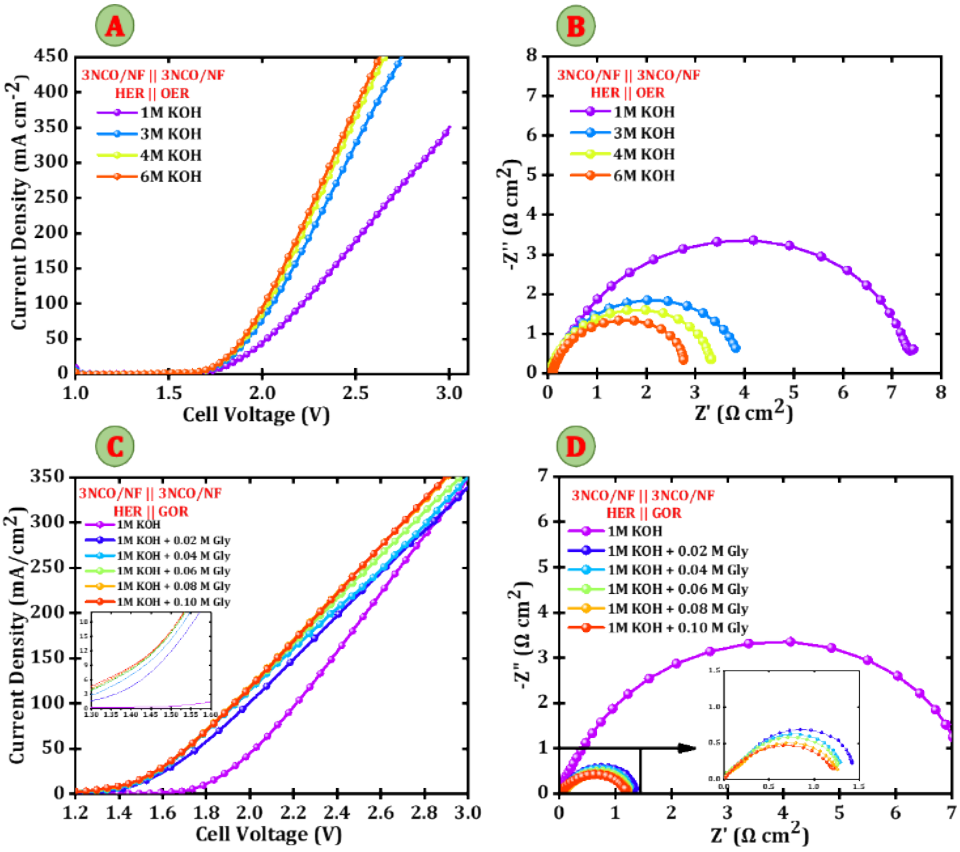

Figure S15 (A) LSV curves (B) Nyquist plots of the 3NCO/NF catalyst in KOH with different concentrations, (C) LSV curves (D) Nyquist plots of the 3NCO/NF catalyst in 1M KOH with varying concentrations of glycerol

Table S1 Comparison of Electrocatalysts for Glycerol Electrooxidation and Formate Production in Alkaline Solution.

Anode	Electrolyte	Potential (V vs. RHE)	References
Nb-Co_3O_4/NF	1M KOH+0.1M GLY	1.19	This work
CuO@Co-MOF	1M KOH+0.1M GLY	1.43	[1]
NiVRu-LDHs NAs/NF)	1 M KOH + 0.1 M GLY	1.40	[2]
CoNi-LDH	1M KOH+0.1M GLY	1.35	[3]
Ni–Mo–N/CFC	1M KOH+0.1M GLY	1.35	[4]
Bi-Co_3O_4	1M KOH+0.1M GLY	1.45	[5]
NC/Ni-Mo-N/NF	1M KOH+0.1M GLY	1.40	[6]
$CuCo_2O_4$	0.1M KOH+0.1M GLY	1.30	[7]
Ni_xBi_{1-x}	1M KOH + 0.1M GLY	1.55	[8]
GDE@AgAu	1 M KOH + 0.1 GLY	1.25	[9]
CoNiB	1 M KOH + 0.1 M GLY	1.42	[10]
HEA-CoNiCuMnMo NPs	1 M KOH + 0.1 M GLY	1.47	[11]
Cu–Cu_2O/CC	1 M KOH + 0.5 M GLY	1.3	[12]
Cu-CuS/BM	0.1 M KOH + 0.1 M GLY	1.45	[13]
Mn-$CoSe_2$/CFC	1 M KOH + 0.1 M GLY	1.27	[14]
Ni_3N-$Ni_{0.2}Mo_{0.8}N$ NWs/CC	1 M KOH + 0.1 M GLY	1.35	[15]
NiV- LDH	1 M KOH + 0.1 M GLY	1.46	[16]
$ZnFe_xCo_{2-x}O_4$	1 M KOH + 0.5 M GLY	1.52	[17]
FeCoO/N-Doped C	1M KOH + 0.1M Glucose	1.29	[18]
Ta-doping NiFe LDH	1M KOH + 0.1M Glucose	1.45	[19]
FexCo2-XP/NF	1M KOH + 0.1M Glucose	1.39	[20]

[1] X. S. X. L. M. C. M. Z. R. Y. R. J. H. Z. Zhefei Zhao, “Electric Field Redistribution Triggered Surface Adsorption and Mass Transfer to Boost Electrocatalytic Glycerol Upgrading Coupled with Hydrogen Evolution,” *Adv Energy Mater*, vol. 14, no. 29, 2024.

[2] X. H. Z. L. Y. C. Y. F. M. C. H. Z. W. W. C. X. G. Z. Y. X. Qizhu Qian, “Electrochemical Biomass Upgrading Coupled with Hydrogen Production under Industrial-Level Current Density,” *Adv Energy Mater*, vol. 35, no. 25, Mar. 2023.

[3] Z. He *et al.*, “Promoting biomass electrooxidation via modulating proton and oxygen anion deintercalation in hydroxide,” *Nat Commun*, vol. 13, no. 1, Dec. 2022, doi: 10.1038/s41467-022-31484-0.

[4] Y. Li, X. Wei, L. Chen, J. Shi, and M. He, “Nickel-molybdenum nitride nanoplate electrocatalysts for concurrent electrolytic hydrogen and formate productions,” *Nat Commun*, vol. 10, no. 1, Dec. 2019, doi: 10.1038/s41467-019-13375-z.

[5] Y. Wang *et al.*, “Efficient Electrocatalytic Oxidation of Glycerol via Promoted OH∗ Generation over Single-Atom-Bismuth-Doped Spinel Co3O4,” *ACS Catal*, vol. 12, no. 19, pp. 12432–12443, Oct. 2022, doi: 10.1021/acscatal.2c03162.

[6] Y. Xu *et al.*, “Integrating electrocatalytic hydrogen generation with selective oxidation of glycerol to formate over bifunctional nitrogen-doped carbon coated nickel-molybdenum-nitrogen nanowire arrays,” *Appl Catal B*, vol. 298, Dec. 2021, doi: 10.1016/j.apcatb.2021.120493.

[7] Xiaotong Han and Song Jin, “Electrocatalytic Oxidation of Glycerol to Formic Acid by CuCo2O4 Spinel Oxide Nanostructure Catalysts,” *ACS Catal*, vol. 10, no. 12, May 2020.

[8] Elena A. Baranova, “Modification of Nickel Surfaces by Bismuth: Effect on Electrochemical Activity and Selectivity toward Glycerol,” *ACS Appl Mater Interfaces*, vol. 12, no. 13, Mar. 2020.

[9] R. Boukil *et al.*, “Enhanced electrocatalytic activity and selectivity of glycerol oxidation triggered by nanoalloyed silver-gold nanocages directly grown on gas diffusion electrodes,” *J Mater Chem A Mater*, vol. 8, no. 18, pp. 8848–8856, May 2020, doi: 10.1039/d0ta01063d.

[10] M. Braun *et al.*, “Cobalt nickel boride as electrocatalyst for the oxidation of alcohols in alkaline media,” *JPhys Energy*, vol. 5, no. 2, Apr. 2023, doi: 10.1088/2515-7655/acbb2a.

[11] Zhenhai Wen, “High Entropy Alloy Electrocatalytic Electrode toward Alkaline Glycerol Valorization Coupling with Acidic Hydrogen Production,” *J Am Chem Soc*, vol. 144, no. 16, 2022.

[12] Suqin Ci, “Energy-saving H2 production from a hybrid acid/alkali electrolyzer assisted by anodic glycerol oxidation,” *Nanoscale*, no. 35, Aug. 2022.

[13] Jiawei DuYang QinTong DouJingmin GeYiping Wang*Xuhui ZhaoFazhi ZhangXiaodong Lei*, “Copper Nanoparticles Dotted on Copper Sulfide Nanosheets for Selective Electrocatalytic Oxidation of Glycerol to Formate,” *ACS Appl Nano Mater*, vol. 5, no. 8, Aug. 2022.

[14] L. Fan *et al.*, “Bifunctional Mn-doped CoSe2 nanonetworks electrode for hybrid alkali/acid electrolytic H2 generation and glycerol upgrading,” *Journal of Energy Chemistry*, vol. 72, pp. 424–431, Sep. 2022, doi: 10.1016/j.jechem.2022.04.027.

[15] X. Liu *et al.*, “Paired formate and H2 productions via efficient bifunctional Ni-Mo nitride nanowire electrocatalysts,” *Journal of Energy Chemistry*, vol. 72, pp. 432–441, Sep. 2022, doi: 10.1016/j.jechem.2022.04.040.

[16] L. Dong, G.-R. Chang, Y. Feng, X.-Z. Yao, and X.-Y. Yu, “Regulating Ni site in NiV LDH for efficient electrocatalytic production of formate and hydrogen by glycerol electrolysis”, doi: 10.1007/s12598.

[17] Haibo WanChencheng DaiLiujun JinSongzhu LuoFanxu MengGao ChenYan DuanChuntai LiuQingfeng Xu*Jianmei Lu*Zhichuan J. Xu*, “Electro-Oxidation of Glycerol to High-Value-Added C1–C3 Products by Iron-Substituted Spinel Zinc Cobalt Oxides,” *ACS Appl Mater Interfaces*, vol. 14, no. 12, Mar. 2022.

[18] M. Tayebi *et al.*, “MOF-Derived FeCoO/N-Doped C Bifunctional Electrode for H2 Production Through Water and Glucose Electrolysis,” *Adv Sustain Syst*, vol. 8, no. 11, Nov. 2024, doi: 10.1002/adsu.202400342.

[19] M. Tayebi *et al.*, “Production of H2 and Glucaric Acid Using Electrocatalyst Glucose Oxidation by the Ta NiFe LDH Electrode,” *ACS Appl Mater Interfaces*, vol. 16, no. 20, pp. 26107–26120, May 2024, doi: 10.1021/acsami.4c02260.

[20] M. Tayebi *et al.*, “MOF-Derived FexCo2-XP/NF Electrocatalysts for Efficient Glucose Oxidation and Water Splitting,” *ACS Appl Energy Mater*, vol. 8, no. 10, pp. 6677–6687, May 2025, doi: 10.1021/acsaem.5c00784.